

Beyond Photon Shot Noise: Chemical Limits in Spectrophotometric Precision

Georg Engelhardt,^{1,*} Dahai He,² and JunYan Luo³

¹*International Quantum Academy, Shenzhen 518048, China*

²*Department of Physics, Xiamen University, Xiamen 361005, China*

³*Department of Physics, Zhejiang University of Science and Technology, Hangzhou 310023, China*

(Dated: January 28, 2026)

In this work, we investigate precision limitations in spectrophotometry (i.e., spectroscopic concentration measurements) imposed by chemical processes of molecules. Using the recently developed Photon-resolved Floquet theory, which generalizes Maxwell-Bloch theory for higher-order measurement statistics, we analyze a molecular model system subject to chemical reactions whose electronic and optical properties depend on the chemical state. Analysis of sensitivity bounds reveals: (i) Phase measurements are more sensitive than intensity measurements; (ii) Sensitivity exhibits three regimes: photon-shot-noise limited, chemically limited, and intermediate; (iii) Sensitivity shows a turnover as a function of reaction rate due to the interplay between coherent electronic dynamics and incoherent chemical dynamics. Our findings demonstrate that chemical properties must be considered to estimate ultimate precision limits in optical spectrophotometry.

I. INTRODUCTION

Spectrophotometry—the measurement of light absorption to determine chemical concentrations—is as one of the most important analytical techniques across scientific disciplines, including medicine, environmental monitoring, biology and engineering [1–9]. At its core lies Beer’s law, relating absorption to concentration. Practical spectrometers face a series of technical limitations, such as sample positioning uncertainties, optical reflections, electronic noise in detectors, and sample preparation inconsistencies [10–14]. Nevertheless, technological improvements in laser spectroscopy—both in intensity and phase measurement—continue to push the boundaries of classical performance [15, 16].

From a more fundamental point of view, quantum optics suggests photon-shot-noise, arising from the quantum nature of light itself, as the fundamental boundary setting the ultimate precision limitation [17, 18]. This perspective has fueled remarkable advances in quantum-enhanced spectroscopy, with squeezed and entangled light sources promising to achieve unprecedented sensitivity [19–24].

In this paper, we argue that the fundamental precision limit in spectrophotometry lies not only in the quantum statistics of light but also in the intrinsic chemical dynamics of the molecules being measured. While single-molecule spectroscopy has long revealed how chemical processes—spectral diffusion, conformational changes, chemical reactions—cause fluctuations in optical properties [25–28], these effects are often dismissed as irrelevant to ensemble measurements where averaging supposedly washes out individual molecular fluctuations. Sophisticated theoretical frameworks, from polaron transformations to hierarchical equations of motion, have been developed to understand these molecular dynamics [29–35],

but their implications for ensemble measurement precision remain largely unexplored.

To investigate this, we develop an operational framework that treats spectrophotometry as an estimation problem, where chemical dynamics directly influence measurement statistics. Our approach leverages the recently developed Photon-resolved Floquet Theory (PRFT) [36], which generalizes the Maxwell-Bloch theory to predict the complete measurement statistics of time-integrated intensities. This enables rigorous application of estimation theory—specifically the Cramér-Rao bound—to determine fundamental sensitivity limits. We analyze a prototypical molecular system undergoing chemical reactions between states with distinct optical properties, a model encompassing conformational changes, configurational transitions, and chemical reactions alike.

The model analysis yields conclusions representative for more sophisticated molecular systems:

- Phase measurements outperform intensity measurements, leveraging coherent quantum effects rather than incoherent absorption. This superiority persists across a wide parameter range.
- As chemical reaction rates vary, measurement sensitivity transitions through three distinct regimes: (i) a *photon-shot-noise limited regime* at fast rates where quantum optical limits prevail; (ii) a *chemically-limited regime* at slow rates where molecular fluctuations dominate; and (iii) an *intermediate regime* where intensity and phase measurements are limited by different mechanisms.
- Sensitivity does not monotonically improve with faster chemical rates. Instead, a turnover emerges where increasing rates initially improve precision by averaging molecular fluctuations, but eventually degrade it by destroying electronic coherence essential for an effective phase-sensitive measurement.

* georg-engelhardt-research@outlook.com

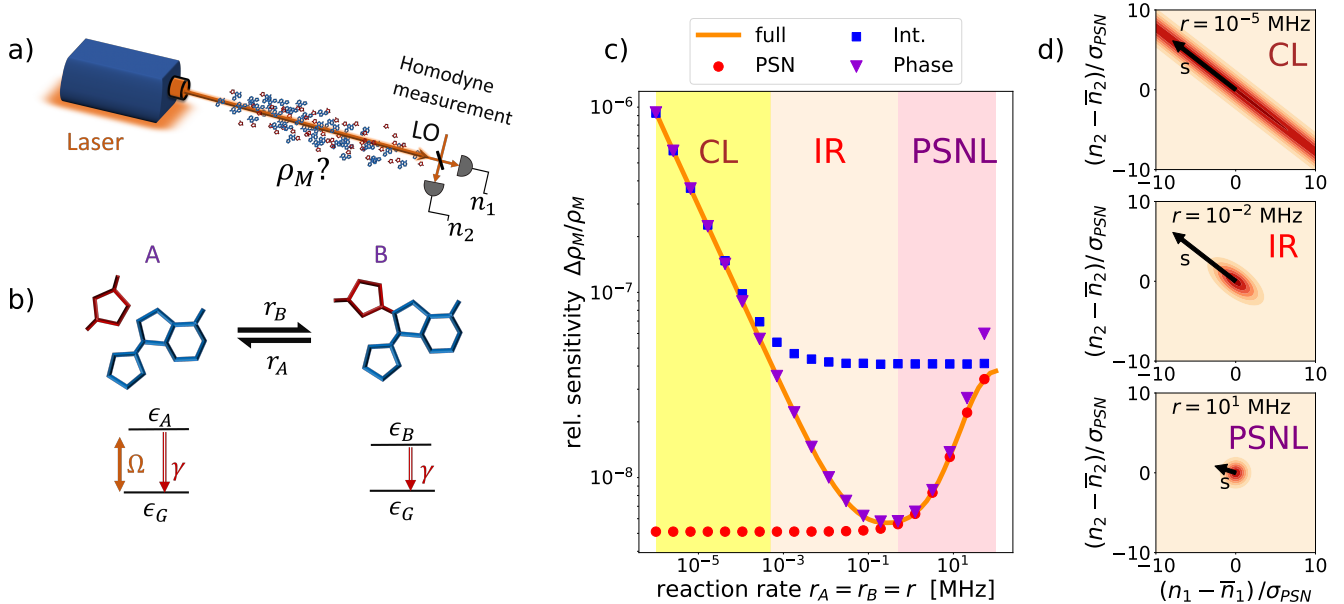


FIG. 1. (a) Prototypical spectrophotometric measurement setup: coherent laser light propagates through a sample containing molecules with concentration ρ_M . The probe laser is measured by a homodyne setup using a local oscillator and two photon detectors. (b) Model molecule undergoing chemical reactions with rates r_A and r_B , with electronic structure depending on the chemical state. (c) Relative sensitivity as a function of chemical reaction rate [Eq. (8), solid line]. Squares and triangles show sensitivity from intensity [Eq. (11a)] and phase [Eq. (11b)] measurements; solid line shows the joint measurement sensitivity; circles show a naive photon-shot-noise estimate. The chemical-limited (CL) regime, the intermediate regime (IR), and the photon-shot-noise limited (PSNL) regimes are highlighted in colors. (d) Probability distributions in the three sensitivity regimes. $\mathbf{s} = \partial_{\rho_M} \bar{\mathbf{n}}$ denotes the signal vector. Parameters are explained in Sec. II A, and $\epsilon_{\Delta} = 40$ MHz.

These findings demonstrate that chemical properties are not merely sample characteristic to be measured, but actively influence the measurement precision itself. They reveal a rich interplay of chemical dynamics and quantum optics that sets the ultimate performance limits.

The remainder of this paper is structured as follows: Sec. II introduces the molecular model and theoretical framework, including the PRFT methodology and sensitivity analysis. Sec. III presents detailed results across the parameter space, explaining the three regimes and their physical origins. Sec. IV summarizes our findings and discusses future research directions. Appendices provide technical details of the PRFT framework and analytical derivations.

II. SYSTEM AND METHODS

A. Molecular system

The experimental setup of a common spectrophotometry device is sketched in Fig. 1(a), in which a laser emits strong coherent light which propagates through a sample containing the molecules whose concentration ρ_M is to be determined. After propagation, the light field is measured by a detector setup. Typically, the measurement is restricted to intensity measurements, but here we envision a homodyne detection, which allows access to both

the intensity and the phase of the probe light.

The molecules exhibit a chemical reaction between two states A and B with distinct electronic and optical properties. The electronic structure of the molecule in each chemical state is sketched in Fig. 1(b), which features distinct excitation energy ϵ_{α} or transition dipole d_{α} depending on state $\alpha = A, B$. The reaction rates between these states are r_A and r_B .

We deploy the PRFT to calculate the probe light modification due to the interaction of the molecules [36]. The molecular dynamics follow the semiclassical quantum master equation

$$\frac{d}{dt}\rho = -\frac{i}{\hbar} [\hat{H}_0, \rho] + \mathcal{L}_{\text{dis}}\rho, \quad (1)$$

in which the Hamiltonian $\hat{H}_0 = \hat{H}_{\varphi=0}$ is given by

$$\hat{H}_{\varphi} = \sum_{\alpha=A,B} \epsilon_{\alpha} |e_{\alpha}\rangle \langle e_{\alpha}| + \hbar \left(\frac{\Omega_{\alpha,\varphi}}{2} |e_{\alpha}\rangle \langle g_{\alpha}| + \text{h.c.} \right). \quad (2)$$

Thereby, $|g_{\alpha}\rangle$ ($|e_{\alpha}\rangle$) denote the ground (excited) state of the molecule in chemical state α . Probe-field induced ground-to-excited-states transitions are described by Rabi frequencies $\Omega_{\alpha,\varphi} = -\mathbf{d}_{\alpha} \cdot \mathbf{E}/\hbar = \frac{d_{\alpha}E}{\sqrt{2}\hbar} (e^{i(\varphi_1 + \pi/4)} + e^{i(\varphi_2 - \pi/4)})$, proportional to the scalar product of state-dependent transition dipoles \mathbf{d}_{α} and the

probe laser electric field \mathbf{E} . The second equality expresses the Rabi frequencies via auxiliary phases φ_k with $k = 1, 2$, allowing to define the photon-flux operators

$$\hat{j}_k = \frac{1}{\hbar} \frac{d}{d\varphi_k} \hat{H}_\varphi. \quad (3)$$

According to the PRFT, these photon-flux operators directly relate to the measurement statistics at detector $k = 1, 2$ in Fig. 1(a).

The Liouvillian in Eq. (1) captures the dissipative dynamics of the molecule

$$\begin{aligned} \mathcal{L}_{\text{dis}}\rho = & \gamma \sum_{\alpha=A,B} D[|g_\alpha\rangle\langle e_\alpha|]\rho \\ & + \sum_{\alpha=A,B} r_\alpha (D[|g_\alpha\rangle\langle g_{\bar{\alpha}}|]\rho + D[|e_\alpha\rangle\langle e_{\bar{\alpha}}|]\rho), \end{aligned} \quad (4)$$

where $D[A]\rho = A\rho A^\dagger - \{A^\dagger A, \rho\}/2$ denotes the common dissipator. The first line describes spontaneous decay from the excited to the ground state with dissipation rate γ . The second line models the chemical reaction dynamics, assuming incoherent dynamics which does not distinguish ground and excited states for simplicity. The notation $\bar{\alpha}$ refers to $\bar{A} = B$ and $\bar{B} = A$.

In the numerical calculations we assume the following realistic parameters: The probe laser has power $P = 1 \text{ mW}$, wavelength $\lambda = 500 \text{ nm}$, and diameter $d = 0.5 \text{ cm}$. The optical transition dipole of the molecules is $d_A = 1 \text{ Debye}$ and $d_B = 0$. These parameters result in a Rabi frequency of $\Omega = 0.95 \text{ MHz}$. The dissipation rate is assumed to be $\gamma = 10 \text{ MHz}$. The total measurement time is $\tau = 1 \text{ s}$.

B. Measurement sensitivity

The homodyne setup in Fig. 1(a) measures the probe field intensities incident to detector $k = 1, 2$ as a function of time. Analysis of this measurement data provides information about the light-matter interaction, such as the density of molecules. The most common observable deployed in this context is the time-integrated intensity operator defined as

$$\hat{n}_k = \frac{\mathcal{A}}{\hbar\omega_p} \int_0^\tau \hat{I}_k(t) dt, \quad (5)$$

where $\hat{I}_k(t)$ is the intensity incident at detector k (in the Heisenberg picture) and τ is the total measurement time. To represent this observable in units of photon numbers, we have multiplied it with the probe laser area \mathcal{A} and divided it by the probe field photon energy $\hbar\omega_p$. The mean and the covariance matrix of this operator are defined as

$$\bar{n}_k = \langle \hat{n}_k \rangle, \quad (6)$$

and

$$[\Sigma^2]_{k,l} = \langle \hat{n}_k \hat{n}_l \rangle - \langle \hat{n}_k \rangle \langle \hat{n}_l \rangle, \quad (7)$$

respectively. To estimate the sensitivity $\Delta X = \langle \Delta \hat{X}^2 \rangle^{1/2}$ of a system parameter X , we can take advantage of the celebrated Cramér-Rao bound [37, 38], which for Gaussian observables reads

$$\langle \Delta \hat{X}^2 \rangle = \left[(\partial_X \bar{\mathbf{n}}) \Sigma^{-2} (\partial_X \bar{\mathbf{n}})^T \right]^{-1}, \quad (8)$$

and requires the evaluation of the means $\bar{\mathbf{n}} = (\bar{n}_1, \bar{n}_2)$ and covariance of the operators \hat{n}_k . For later purpose, we also introduce $\hat{n}_\pm = \hat{n}_1 \pm \hat{n}_2$.

After mixing the probe field with the coherent local oscillator field at the beam splitter [see Fig. 1(a)], we find

$$\begin{pmatrix} \bar{n}_1 \\ \bar{n}_2 \end{pmatrix} = \bar{n}_+ \begin{pmatrix} \cos^2(\frac{\pi}{4} + \frac{\varphi - \varphi_{\text{LO}}}{2}) \\ \sin^2(\frac{\pi}{4} + \frac{\varphi - \varphi_{\text{LO}}}{2}) \end{pmatrix}, \quad (9)$$

where \bar{n}_+ equals the sum of photons in the probe field \bar{n}_p (after the interaction with the molecules) and the local oscillator \bar{n}_{LO} , and we assume that $\bar{n}_{\text{LO}} = \bar{n}_p = \bar{n}_+/2$. The probe field (local oscillator) has mean phase $\bar{\varphi}$ (φ_{LO}). Choosing the local oscillator phase such that $\bar{n}_1 = \bar{n}_2$, we find

$$\partial_X \bar{\mathbf{n}}^T = \bar{n}_p \frac{d\bar{\varphi}}{dX} \begin{pmatrix} 1 \\ -1 \end{pmatrix} + \frac{d\bar{n}_p}{dX} \begin{pmatrix} 1 \\ 1 \end{pmatrix}. \quad (10)$$

Restricting the data analysis to either intensity or phase measurement, the corresponding sensitivity bounds are given by

$$\langle \Delta X^2 \rangle_{\mathcal{I}} = \left(\frac{d\bar{n}_p}{dX} \right)^{-2} \Sigma_+^2, \quad (11a)$$

$$\langle \Delta X^2 \rangle_{\varphi} = \left(\bar{n}_p \frac{d\bar{\varphi}}{dX} \right)^{-2} \Sigma^2, \quad (11b)$$

where $\Sigma_\pm^2 = v_\pm \Sigma^2 v_\pm^T$ with $v_+ = (1, 1)$ and $v_- = (1, -1)$ are the variance of the operators \hat{n}_\pm .

C. Evaluation

To evaluate Eq. (8), we need to calculate the first two cumulants of the measurement statistics. We assume a sufficiently weak probe field ensuring the validity of Beer's absorption law,

$$\bar{n}_p(z) = \bar{n}_{p,0} e^{-\rho_M \mathcal{S}_+ z}, \quad (12)$$

where z is the propagation distance, $\bar{n}_{p,0} = \bar{n}_p(z=0)$ is the initial photon number of the probe field, ρ_M is the molecular density, and \mathcal{S}_+ is the absorption cross section.

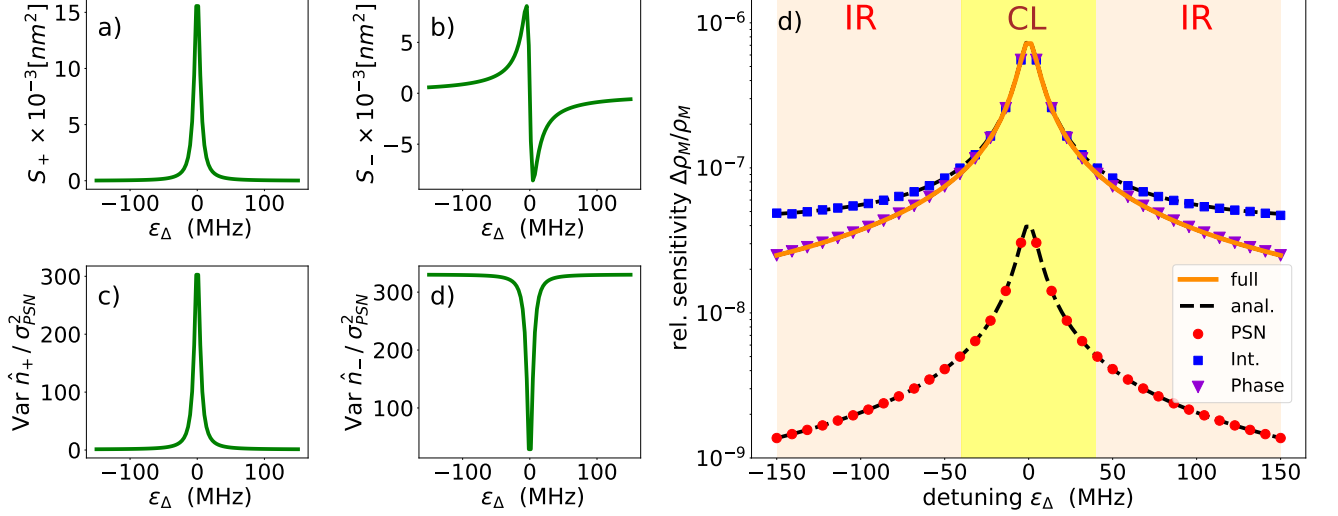


FIG. 2. (a) Absorption cross section as function of detuning for the model system in Eq. (1) evaluated using Eq. (14) for $\tau \rightarrow \infty$. (b) Phase-shift cross section evaluated using Eq. (14). (c) Variance of \hat{n}_+ of the time-integrated intensity measurements in Eq. (19b). (d) Variance of \hat{n}_- calculated using the same equation. (e) Relative sensitivity as a function of detuning as predicted by full measurement statistics [Eq. (8), solid line], intensity measurement [squares, Eq. (11a)], phase measurement [triangles, Eq. (11b)] and a simple photon-shot noise estimate (circles). Analytical calculations are depicted by a black dashed line. Overall parameters are explained in Sec. II A, and $r_A = r_B = 10^{-4}$ MHz.

The phase shift of the probe field fulfills

$$\bar{\varphi} = \rho_M \mathcal{S}_- z, \quad (13)$$

where \mathcal{S}_- is the phase-shift cross section. These cross sections fulfill $\mathcal{S}_\pm = \mathcal{S}_1 \pm \mathcal{S}_2$ with

$$\mathcal{S}_k = \frac{1}{\mathcal{J}\tau} \int_0^\tau \langle \hat{j}_k(t) \rangle dt, \quad (14)$$

where we have defined the photon-number intensity $\mathcal{J} = \mathcal{I}/\hbar\omega_p = \bar{n}_p/(\mathcal{A}\tau)$ in terms of the common intensity \mathcal{I} . Relations (12)-(14) can be derived using the PRFT as shown in Appendix A.

Likewise, the covariance matrix in the weak-probe-field regime is given by

$$\Sigma^2(z) = \Sigma_0^2 e^{-2\rho_M \mathcal{S}_+ z} + \int_0^z e^{-2\rho_M \mathcal{S}_+(z-z')} \mathbf{D}_{\mathcal{J}(z')} dz', \quad (15)$$

where $\Sigma_0^2 = \bar{n}_{p,0} \mathbf{1}$ is the initial covariance matrix, and the diffusion matrix can be calculated via

$$[\mathbf{D}_{\mathcal{J}}]_{k,l} = \rho_M \mathcal{A} \int_0^\tau \int_0^\tau \langle \Delta \hat{j}_k(t_1) \Delta \hat{j}_l(t_2) \rangle dt_1 dt_2, \quad (16)$$

where $\Delta \hat{j}_k(t) = \hat{j}_k(t) - \langle \hat{j}_k(t) \rangle$. This relation is valid for a coherent local oscillator with $\bar{n}_{\text{LO}} = \bar{n}_p(z)$ obeying Poisson statistics.

To make progress, we assume the following expansion of the diffusion matrix in orders of the photon-number

intensity

$$\mathbf{D}_{\mathcal{J}} = \rho_M \tau \mathcal{A} \sum_{m=1}^{\infty} \frac{1}{m!} \mathbf{D}^{(m)} \mathcal{J}^m. \quad (17)$$

Our analysis for the molecular model in Eq. (1) will show that the diffusion matrix is fully characterized by the first two expansion orders. Evaluating Eq. (15) using Eq. (17), we find

$$\begin{aligned} \Sigma^2 &= \Sigma_0^2 e^{-2\rho_M \mathcal{S}_+ z} \\ &+ \bar{n}_{p,0} \frac{\mathbf{D}^{(1)}}{\mathcal{S}_+} (e^{-\rho_M \mathcal{S}_+ z} - e^{-2\rho_M \mathcal{S}_+ z}) \\ &+ e^{-2\rho_M \mathcal{S}_+ z} \bar{n}_{p,0} \mathcal{J}_0 \rho_M \mathbf{D}^{(2)} z, \end{aligned} \quad (18)$$

where $\mathcal{J}_0 = \bar{n}_{p,0}/(\mathcal{A}\tau)$ and we have neglected terms of order \mathcal{J}^m with $m \geq 3$.

In this work, we consider optical thick samples such that the propagation length z maximizes the signal intensity $\partial_{\rho_M} \bar{n}_+(z)$, that is, for $z = z_{\text{opt}} = 1/(\rho_M \mathcal{S}_+)$. In doing so, we find that

$$\frac{\partial \bar{n}_p}{\partial \rho_M} = \frac{\bar{n}_{p,0}}{e \rho_M}, \quad \frac{\partial \bar{\varphi}}{\partial \rho_M} = \frac{\mathcal{S}_-}{\rho_M \mathcal{S}_+} \quad (19a)$$

$$\Sigma_\pm^2 = \frac{\Sigma_{\pm,0}^2}{e^2} + \bar{n}_{p,0} \frac{\mathbf{D}_\pm^{(1)}}{\mathcal{S}_+} \left(\frac{1}{e} - \frac{1}{e^2} \right) + \bar{n}_{p,0} \frac{\mathcal{J}^{(0)} \mathbf{D}_\pm^{(2)}}{e^2 \mathcal{S}_+}, \quad (19b)$$

which can be used to evaluate Eq. (11). Thereby, we also defined $\mathbf{D}_\pm = v_\pm \mathbf{D}^{(m)} v_\pm^T$.

III. RESULTS

We are now in position to analyze the molecular model in Eq. (1). For simplicity, we assume that the transition dipole matrix elements of state B are zero. Figure 2(a) and (b) depict the absorption and phase-shift cross sections as a function of the probe-field detuning, respectively. The absorption cross section displays the common absorption dip at zero detuning, while the phase-shift cross section exhibits the well-known dispersive curve. As shown in Appendix B, in an adiabatic regime for which $\gamma \ll r_A, r_B$, the cross sections are given by

$$\mathcal{S}_{\pm} = p_A \mathcal{S}_{\pm|A} + p_B \mathcal{S}_{\pm|B}, \quad (20)$$

where $p_{\alpha} = r_{\alpha}/(r_A + r_B)$ is the stationary probability to be in the chemical state α . The cross sections conditioned on state $\alpha = A$ are

$$\begin{aligned} \mathcal{S}_{+|A} &= \frac{1}{2} \frac{\gamma \beta^2}{4\epsilon_{\Delta}^2 + \gamma^2}, \\ \mathcal{S}_{-|A} &= \frac{1}{2} \frac{2\epsilon_{\Delta} \beta^2}{4\epsilon_{\Delta}^2 + \gamma^2}, \end{aligned} \quad (21)$$

with $\epsilon_{\Delta} = \epsilon/\hbar - \omega_p$ and $\beta = d_A \sqrt{2\hbar\omega_p/\epsilon_0 c}$ (speed of light c , dielectric constant ϵ_0), while the cross sections $\mathcal{S}_{\pm|B} = 0$ as $d_B = 0$. Evidently, a finite d_B would give rise to a double peak structure of the cross sections according to Eq. (20).

An example for the variances of the observables \hat{n}_+ and \hat{n}_- is depicted in Fig. 2(c) and (d), respectively, in units of the $\sigma_{\text{PSN}}^2 \equiv 2\bar{n}_p(z_{\text{opt}})$, which can be regarded as a naive photon-shot noise estimate neglecting the noise added by the light-matter interaction. We observe in Fig. 2(c) and (d) that the full variance can drastically exceed this simple shot-noise estimate by more than two orders of magnitude, emphasizing the importance to take the noise added by the light-matter interaction into account. Moreover, we also observe that the variance of \hat{n}_+ and \hat{n}_- behave complementary, that is, the \hat{n}_+ variance is large close to resonance, while the \hat{n}_- variance is large for off-resonance detunings, which will be corroborated with analytical calculations below.

In the adiabatic regime, the matrix elements of the diffusion matrix are given by

$$\begin{aligned} [\mathcal{D}_{\mathcal{J}}]_{k,l} &= p_A D_{k,l|A} + p_B D_{k,l|B} \\ &+ \rho_M \tau \mathcal{A} \mathcal{J}^2 t_R p_A p_B (\mathcal{S}_{k|A} - \mathcal{S}_{k|B}) (\mathcal{S}_{l|A} - \mathcal{S}_{l|B}), \end{aligned} \quad (22)$$

as shown in Appendix B, where we have defined the effective reaction time as

$$t_R = \frac{1}{r_A + r_B}. \quad (23)$$

The first line terms of Eq. (22) represent diffusion matrices conditioned on the state $\alpha = A, B$ weighted by the

stationary state probabilities p_{α} . This term dominates for small t_R . The simplicity of the molecular model allows for an evaluation of the terms $D_{k,l|A}$, which are explicitly given in Eq. (B9). Moreover, the adiabatic diffusion terms $D_{\pm}^{(m)}$ related to intensity and phase measurements are given by

$$\begin{aligned} D_{+|A}^{(1)} &= D_{-|A}^{(1)} = \frac{\gamma \beta^2}{4\epsilon_{\Delta}^2 + \gamma^2}, \\ D_{+|A}^{(2)} &= \frac{\beta^4 \gamma (8\epsilon_{\Delta}^2 - 6\gamma^2)}{(4\epsilon_{\Delta}^2 + \gamma^2)^3}, \\ D_{-|A}^{(2)} &= \frac{2\beta^4}{\gamma (4\epsilon_{\Delta}^2 + \gamma^2)} - \frac{8\epsilon_{\Delta}^2 (4\epsilon_{\Delta}^2 + 5\gamma^2) \beta^4}{\gamma (4\epsilon_{\Delta}^2 + \gamma^2)^3}. \end{aligned} \quad (24)$$

However, numerical analysis shows that these terms hardly contribute to the variance as compared to the photon-shot-noise σ_{PSN}^2 . Thus we focus on the term in the second line of Eq. (22) in the following. We analyze the measurement statistics in three regimes, namely a photon-shot-noise limited regime for small t_R , a chemically-limited regime for large t_R , and an intermediate regime for modest t_R .

A. Photon-shot-noise-limited regime

In the photon-shot-noise-limited (PSNL) regime, the measurement variance is dominated by the first two lines in Eq. (18). Comparison of Eqs. (21) and (24) reveals that $D_{\pm}^{(1)} = 2\mathcal{S}_{\pm}$. For this reason, we directly find that

$$\frac{\Sigma_{\pm}^2}{\sigma_{\text{PSN}}^2} \approx 1, \quad (25)$$

which means that the measurement statistics is given by the photon-shot noise.

The measurement sensitivity in the PSNL regime is highlighted in Fig. 1(b) in the large reaction rate regime, where the sensitivity estimated by the full Cramér-Rao bound in Eq. (8) (solid line) coincides with the photon-shot noise estimate (circles). This agreement shows that noise added by the light-matter interaction has a relatively minor impact. For relatively small $r_A = r_B = r$ within this regime, the measurement sensitivity is dominated by the phase measurement, which exceeds the intensity measurement due to the favorable scaling of \mathcal{S}_- with ϵ_{Δ} in comparison to \mathcal{S}_+ . This scaling is a result of the coherent nature of the phase shift, which contrast the incoherent dynamics characterizing the absorption. Only for very large $r \approx 10^2$ MHz does the full measurement sensitivity comes from the intensity measurement. Here, rapid incoherent transitions between the chemical states destroy any electronic coherence in A , which is necessary to produce a phase shift, but do not influence the absorption.

Because of the Poisson statistics of the initial probe

light, the relative concentration measurement sensitivity is ultimately limited by

$$\frac{\Delta\rho_M}{\rho_M} \rightarrow \sqrt{\frac{e}{\bar{n}_{p,0}}} \quad (26)$$

in the $r \rightarrow \infty$ limit, obtained by combining Eqs. (11), (19a), and (25) for the intensity measurement. Thus, the relative sensitivity is only limited by the total number of photons deployed during the measurement. We remark that this does not imply that the measurement sensitivity can be arbitrarily improved by a large probe laser intensity, as our analysis is restricted to weak probe fields. However, as $\bar{n}_p^{(0)} \propto \tau$, the measurement precision improves with the square root of the measurement time.

We depict the probability distribution in the PSNL regime as a function of the photon numbers n_k measured at detector k in the lower panel of Fig. 1(d), in which the probability distribution is equal along the directions $n_+ = n_1 + n_2$ and $n_- = n_1 - n_2$. Despite the relatively small noise, the sensitivity is low, as the signal vector $\mathbf{s} = \partial_{\rho_M} \bar{\mathbf{n}}$ is small, which is a consequence of the rapid chemical transitions destroying electronic coherence in state A .

B. Chemically-limited regime

For small r_A, r_B , inspection of Eq. (18) and Eq. (22) reveals that the measurement variance is dominated by the second term proportional to t_R in Eq. (23). Assuming that $d_B = 0$, we find

$$\frac{\Sigma_{\pm}^2}{\sigma_{\text{PSN}}^2} \rightarrow \frac{\bar{n}_{p,0}}{e} \frac{p_B}{p_A} \frac{\mathcal{S}_{\pm|A}^2}{\mathcal{S}_{+|A} \mathcal{A}} \frac{t_R}{\tau}, \quad (27)$$

expressing the variance in terms of the cross sections $\mathcal{S}_{\pm|A}$. We find that this term is suppressed for $p_A \gg p_B$, that is, for $r_A \gg r_B$. This defines a parameter regime, in which the sensitivity is chemically limited (CL), which is marked in Fig. 1(c).

Inserting the cross-section expressions of Eq. (21) into Eq. (27) yields

$$\begin{aligned} \frac{\Sigma_{+}^2}{\sigma_{\text{PSN}}^2} &\rightarrow \frac{p_B}{p_A} \frac{\gamma \Omega^2}{4\epsilon_{\Delta}^2 + \gamma^2} \frac{t_R}{e}, \\ \frac{\Sigma_{-}^2}{\sigma_{\text{PSN}}^2} &\rightarrow \frac{p_B}{p_A} \frac{4\epsilon_{\Delta}^2 \Omega^2}{\gamma (4\epsilon_{\Delta}^2 + \gamma^2)} \frac{t_R}{e} \end{aligned} \quad (28)$$

for the intensity and phase measurement variants, respectively, which reflects the functional form in Fig. 2(c) and (d). For an absorption measurement with $\epsilon_{\Delta} = 0$, and for a phase measurement with $\epsilon_{\Delta} \gg \gamma$, both cases scale $\frac{\Sigma_{\pm}^2}{\sigma_{\text{PSN}}^2} \propto \Omega^2 t_R / \gamma$, which allows to estimate the relative contribution of the chemical uncertainty to the total measurement noise.

Interestingly, using either expression in Eq. (28)

to evaluate the concentration measurement sensitivity Eq. (11), we find

$$\frac{\Delta\rho_M}{\rho_M} \rightarrow \sqrt{\frac{p_B}{p_A} \frac{\mathcal{S}_{+}}{\mathcal{A}} \frac{t_R}{\tau}}, \quad (29)$$

which depends on the ratio of the stationary probabilities, $\frac{p_B}{p_A}$, the ratio of the absorption and probe field laser cross section, as well as the ratio of the effective chemical reaction time and the total measurement time.

The corresponding probability distribution is depicted in the upper panel Fig. 1(d). While not fully aligned with the direction n_- , the probability distribution is more spread in the direction n_- than in the direction n_+ , as for this off-resonance sensing the phase shift has a more substantial impact on the probe field than the absorption. The signal vector \mathbf{s} is parallel to the long axes of the probability ellipsoid, which results from the quadratic dependence of the diffusion matrix in Eq. (22) on the cross sections $\mathcal{S}_{k|\alpha}$ for large t_R .

C. Intermediate regime

Between the PSNL regime for short t_R and the CL regime for long t_R , there is an intermediate regime (IR), which is marked in Fig. 1(c). Here, the intensity-measurement variance is dominated by the photon-shot noise, while the phase-measurement variance is dominated by the chemically-induced measurement noise. As the phase-measurement is overall more sensitive than the absorption measurement, the full measurement sensitivity coincides with the sensitivity of the phase measurement.

The probability distribution in the intermediate regime is depicted in the middle panel Fig. 1(d). While the distribution clearly expands in the n_- direction related to the phase measurement, the extension in the n_+ hardly exceeds the photon-shot noise contribution (see bottom panel for comparison), reflecting that the absorption measurement is limited by the photon-shot noise, while the phase measurement is limited by the chemical noise.

D. Detuning dependence

As the detuning is a crucial control parameter, we discuss here in detail the sensitivity dependence on the detuning, which is depicted in Fig. 2(d) for a small $r_A = r_B = 10^{-4}$ MHz. The full sensitivity [Eq. (8)] is depicted by an orange solid line, while the sensitivity for the intensity measurement [Eq. (11a)], the phase measurement [Eq. (11b)] and for the photo-shot-noise estimate are depicted by markers. All sensitivity estimates peak at $\epsilon_{\Delta} = 0$, and then improve monotonically with increasing detuning. Thereby, we can identify two of the three sensitivity regimes:

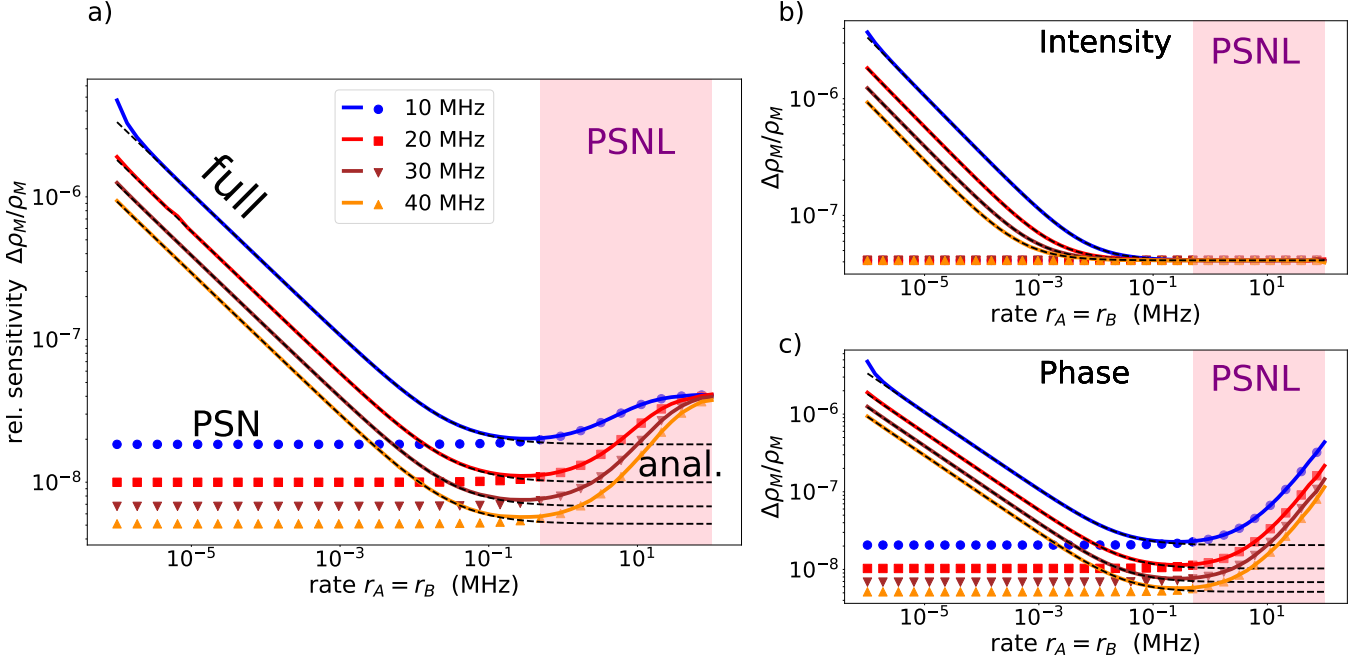


FIG. 3. Relative sensitivity as a function of reaction rate evaluated using Eqs. (8), (18), and (19a). Solid lines depict sensitivity bounds determined by the full measurement statistics for various detunings, while markers show the sensitivity bounds predicted by the photon-shot-noise estimate. Dashed lines show the analytical calculations. (b) and (c) depict the same as (a), but restricted to intensity and phase measurements, respectively. Overall parameters are explained in Sec. II A.

For small detuning, we find that the full sensitivity, intensity-measurement sensitivity, and the phase-measurement sensitivity agree with each other, and fall short of the photon-shot-noise estimate. Consequently, the system is in the chemically-limited regime. For large detuning $|\epsilon_\Delta| > 50$ MHz, the sensitivity offered by the intensity measurement is larger than the phase-measurement sensitivity, which still agrees with the full sensitivity. In this regime, the intensity-measurement noise is dominated by the photon-shot noise, such that the system is in the intermediate regime.

To further investigate the interplay between rate and detuning, we depict the relative sensitivity as a function of reaction rate for various detunings in Fig. 3(a). For comparison, we added the sensitivity predicted by the photon-shot-noise estimate by markers in the same colors. For all detunings, we observe a turnover as a function of the reaction rate, that is, an improving sensitivity for small reaction rates, and a deteriorating sensitivity for large reaction rates. As in the latter case the photon-shot-noise estimate agrees with the full sensitivity, we conclude that the system is in the PSNL regime.

To better understand the contributions of the intensity and the phase measurement to the full sensitivity, we depict the respective sensitivity estimates in Figs. 3(b) and (c), respectively. The intensity-measurement sensitivity exhibits a monotonic decay for all detuning values. Beyond a detuning-specific reaction rate, the sensitivity saturates and agrees with the sensitivity predicted by the

photon-shot-noise estimate. As this specific value does depend on the detuning, we do not highlight the intermediate regime in the panels of Fig. 3. Comparison of panels (a), (b) and (c) reveals that the turnover in the full sensitivity is inherited by the turnover in the phase-measurement sensitivity. In contrast to the intensity-measurement, the phase-measurement allows for a clear identification of the onset of the photon-shot-noise limited regime, which is independent of the detuning.

IV. CONCLUSIONS

This work reveals that the ultimate precision of optical spectrophotometry is fundamentally constrained not only by the quantum statistics of light but also by the intrinsic chemical dynamics of the target molecules. By treating spectrophotometry as an estimation problem within the framework of the Photon-resolved Floquet Theory (PRFT), we have quantified how chemical processes directly shape measurement statistics and set ultimate sensitivity bounds.

First, phase-sensitive measurements consistently outperform intensity measurements by leveraging coherent quantum effects. Second, the analysis identifies three distinct sensitivity regimes— (i) a regime in which the sensitivity is limited by the photon-shot noise for large reaction rates; (ii) a regime in which the sensitivity is limited by chemical processes for small reaction rates; (iii)

an intermediate regime in which the intensity measurement is limited by photon-shot noise, while the phase-measurement is limited by chemical processes. Third, the interplay between coherent and incoherent dynamics gives rise to a turnover in the sensitivity as a function of the reaction rate. Our analysis demonstrates that the ultimate limit in spectroscopic concentration measurements is set by an interplay between quantum optics and chemical dynamics. Ignoring the noise introduced by the light-matter interaction leads to an overly optimistic estimate of the achievable precision.

While our analysis using a simplified four-state model provides fundamental insights, it naturally opens avenues for future work. Incorporating coherent chemical transitions (e.g., via polaron-transformed master equation [31, 39–43], HEOM methods [33], or advanced quantum master equation approaches [44, 45]), photo-induced reaction pathways, and effects like rotational averaging or Doppler broadening into the PRFT framework will be essential for predicting precision limits in realistic, complex molecular systems. This work establishes a crucial step toward a complete quantum-mechanical theory of spectrophotometric precision, where the molecule is treated not as a static object but as a dynamic quantum entity whose fluctuations determine the ultimate measurement sensitivity.

ACKNOWLEDGMENTS

G.E. acknowledges support by the National Natural Science Foundation of China (NSFC) (Grant No. W2432004). J.Y.L. acknowledges the support from the NSFC (Grant No. 11774311). D.H. acknowledges financial support from the NSFC (Grants No. 12475039) and the Guangdong Basic and Applied Basic Research Foundation (Grant No. 2025A1515010350).

Appendix A: Photon-resolved Floquet theory

The PRFT adaptation to spectroscopy can be regarded as an extension of the celebrated Maxwell-Bloch theory capable of predicting the measurement statistics of time-integrated intensity measurements [36]. Similar to the Maxwell-Bloch theory, the PRFT relies on the solution of semiclassical equations of motion of the matter system to retrieve the relevant information about the photon statistics of an electromagnetic probe field. Here, we consider the system in Sec. II A assuming a probe field propagating through an ensemble of molecules and a homodyne measurement with a coherent local oscillator fulfilling $\bar{n}_{\text{LO}} = \bar{n}_p(z)$. To obtain the photon statistics at the photon detectors $k = 1, 2$, we solve a two-sided quantum master equation of the form

$$\frac{d}{dt}\rho_{\chi} = -i \left[H_{\varphi+\frac{\chi}{2}} \rho_{\chi} - \rho_{\chi} H_{\varphi-\frac{\chi}{2}} \right] + \mathcal{L}_{\text{dis}} \rho_{\chi}, \quad (\text{A1})$$

where the Hamiltonian is defined in Eq. (2) and depends on the so-called counting fields $\chi = (\chi_1, \chi_2)$. Using the time-integrated and counting-field dependent density matrix, we define the cumulant-generating function via

$$\mathcal{K}_{\chi} = \log \text{tr} [\rho_{\chi}]. \quad (\text{A2})$$

In terms of the cumulant-generating function, we can construct flow equations for all relevant observable in spectroscopy, such as for the total photon number and the mean phase, which read

$$\begin{aligned} \frac{d\bar{n}_+}{dz} &= \partial_z \bar{n}_2 + \partial_z \bar{n}_1, \\ \frac{d\bar{\varphi}}{dz} &= \frac{\partial_z \bar{n}_2 - \partial_z \bar{n}_1}{\bar{n}_+}. \end{aligned} \quad (\text{A3})$$

Thereby, $\partial_z \bar{n}_k$ refers to the derivatives of the mean photon number \bar{n}_k with respect to the propagation distance z and can be evaluated via

$$\partial_z \bar{n}_k = \rho_M \mathcal{A} \partial_{\chi_k} \mathcal{K}_{\chi=0}(z). \quad (\text{A4})$$

To evaluate Eqs. A3, we further assume that

$$\partial_z \bar{n}_k = \rho_M \mathcal{S}_k \bar{n}_+ \quad (\text{A5})$$

with a constant \mathcal{S}_k . This condition is typically fulfilled in the weak probe field regime. Using methods introduced in Ref. [36] it is also possible to show that \mathcal{S}_k can be represented in the integral form of Eq. (14). Integration of Eqs. (A3) now directly leads to Eqs. (12) and (13).

Likewise, one can construct a flow equation for the covariance matrix related to time-integrated photon numbers, which reads

$$\frac{d}{dz} \boldsymbol{\Sigma}^2 = \mathbf{D}_{\bar{n}} + \mathbf{C}_{\bar{n}} \boldsymbol{\Sigma}^2 + \boldsymbol{\Sigma}^2 \mathbf{C}_{\bar{n}}, \quad (\text{A6})$$

and has to be solved with initial condition $\boldsymbol{\Sigma}^2(0) = \bar{n}_{p,0} \mathbf{1}$. The coefficients can be expressed in terms of the cumulant-generating function as

$$\begin{aligned} [\mathbf{D}_{\bar{n}}]_{k,l} &= \rho_M \mathcal{A} \partial_{\chi_k} \partial_{\chi_l} \mathcal{K}_{\chi=0}(z), \\ [\mathbf{C}_{\bar{n}}]_{k,l} &= \rho_M \mathcal{A} \partial_{\bar{n}_k} \partial_{\chi_l} \mathcal{K}_{\chi=0}(z) - \frac{1}{2} \frac{d\bar{\varphi}}{dz} \hat{\Xi}, \end{aligned} \quad (\text{A7})$$

where $\hat{\Xi} = \hat{\sigma}_x + i\hat{\sigma}_y$. In this form, the flow equation describes the measurement statistics deploying a coherent local oscillator with Poisson photon statistics and $\bar{n}_{\text{LO}} = \bar{n}_p(z)$, with its phase chosen such that $\bar{n}_1 = \bar{n}_2$ [36]. Finally, under the assumption in Eq. (A5), one can show that

$$\mathbf{C}_{\bar{n}} = \rho_M \mathcal{S}_+ \mathbf{1}, \quad (\text{A8})$$

which allows for an analytical integration of Eq. (15) yielding Eq. (18).

Appendix B: Spectroscopic properties of the molecule in the adiabatic regime

1. Adiabatic approximation

In this appendix, we derive the expression for the spectroscopic properties of the molecular system in Sec. II A, without explicitly specifying the electronic properties in each state. As the chemical transition described by the second line in Eq. (4) is incoherent, we can neglect the corresponding coherence matrix elements in the density matrix and represent it as $\rho = (\rho_A, \rho_B)$. In this representation, the two-sided master equation in Eq. (A1) reads

$$\frac{d}{dt} \rho_{\chi} = \begin{pmatrix} \mathcal{L}_{\chi|A} & \mathcal{R}_{AB} \\ \mathcal{R}_{BA} & \mathcal{L}_{\chi|B} \end{pmatrix} \rho_{\chi}, \quad (\text{B1})$$

where $\mathcal{L}_{\chi|\alpha}$ describes the dynamics within one of the chemical states $\alpha = A, B$, and $\mathcal{R}_{AB}, \mathcal{R}_{BA}$ represents the transition between the two chemical states.

Now we assume the following adiabatic ansatz for the counting-field dependent density matrix

$$\rho_{\chi} = \left(p_{A,\chi} \rho_{\chi|A}^{(0)}, p_{B,\chi} \rho_{\chi|B}^{(0)} \right), \quad (\text{B2})$$

where

$$\mathcal{L}_{\chi|\alpha} \rho_{\chi|\alpha}^{(0)} = \mathcal{K}_{\chi|\alpha} \rho_{\chi|\alpha}^{(0)}, \quad (\text{B3})$$

such that $\mathcal{K}_{\chi|\alpha}$ is the eigenvalue of $\mathcal{L}_{\chi|\alpha}$ with the largest real part. Introducing the notation $\mathbf{p} = (p_{A,\chi}, p_{B,\chi})$, inserting Eq. (B2) into the master equation in Eq. (B1), and taking the partial trace over the electronic degrees of freedom, we obtain

$$\frac{d}{dt} \mathbf{p} = \begin{pmatrix} \mathcal{K}_{\chi|A} & r_A \\ r_B & \mathcal{K}_{\chi|B} \end{pmatrix} \mathbf{p}, \quad (\text{B4})$$

where we have approximated $\text{tr} \left[\rho_{\chi|\alpha}^{(0)} \right] \approx 1$ and $\text{tr} \left[\mathcal{R}_{AB} \rho_{\chi|A}^{(0)} \right] \approx r_A$, and $\text{tr} \left[\mathcal{R}_{BA} \rho_{\chi|B}^{(0)} \right] \approx r_B$. This form is valid if r_A, r_B is smaller than the dissipative dynamics within each $\mathcal{L}_{\chi|\alpha}$, such that the stationary state of each chemical state α (represented by $\mathcal{K}_{\chi|\alpha}$) can be approached before the system undergoes a chemical transition.

The statistics for long measurement times τ is determined by the dominating eigenvalue of the Liouvillian in Eq. (B4), which explicitly reads

$$\begin{aligned} \lambda_{\chi} = & \frac{1}{2} (\mathcal{K}_{\chi|A} + \mathcal{K}_{\chi|B} - r_A - r_B) \\ & + \frac{1}{2} \sqrt{(\mathcal{K}_{\chi|A} - \mathcal{K}_{\chi|B} - r_A + r_B)^2 + 4r_A r_B}, \end{aligned} \quad (\text{B5})$$

such that

$$\mathcal{K}_{\chi} = \lambda_{\chi} \tau \quad (\text{B6})$$

is the asymptotic cumulant-generating function for $\tau \rightarrow \infty$, which can be used to evaluate (A4) and (A7).

Taking the first derivatives with respect to χ_k and using Eq. (B4), we find

$$\partial_z \bar{n}_k = p_A \partial_z \bar{n}_{k|A} + p_B \partial_z \bar{n}_{k|B}, \quad (\text{B7})$$

where $\partial_z \bar{n}_{k|\alpha} = -i \rho_M \mathcal{A} \partial_{\chi_k} \mathcal{K}_{\chi=0|\alpha} \tau$ is the photon-flux conditioned on the chemical state α and $p_{\alpha} = r_{\alpha} / (r_A + r_B)$ are the stationary probabilities. Using now Eqs. (A4) and (A5), we finally arrive at Eq. (20).

To evaluate the diffusion matrix in Eq. (A7), we derive Eq. (B6) two times with respect to the counting fields and obtain

$$\begin{aligned} D_{k,l} = & p_A D_{k,l|A} + p_B D_{k,l|B} \\ & + \frac{t_R p_A p_B}{\rho_M \tau \mathcal{A}} (\partial_z \bar{n}_{k|A} - \partial_z \bar{n}_{k|B}) (\partial_z \bar{n}_{l|A} - \partial_z \bar{n}_{l|B}), \end{aligned} \quad (\text{B8})$$

where $D_{k,l|\alpha} = -\rho_M \mathcal{A} \partial_{\chi_k} \partial_{\chi_l} \mathcal{K}_{\chi=0|\alpha} \tau$ are the diffusion matrix elements conditioned on the chemical state α . Using again Eq. (A5), we eventually obtain Eq. (22).

2. Diffusion matrix elements conditioned on the chemical state

To fully evaluate Eq. (B8), we must find a closed expression for the diffusion-matrix elements conditioned on the chemical state α . As we assumed that $d_B = 0$, we only have to evaluate the elements for $\alpha = A$. Therefore, we refer to Ref. [36] which has derived these matrix elements already for a dissipative two-level system. In the weak-probe-field regime for which $\Omega^2 / \gamma^2 \ll 1$, the matrix elements become

$$\begin{aligned} D_{k,l|A} = & \rho_M \mathcal{A} \left[\frac{a_0^{(kl)}}{a_1} + \frac{2a_2 a_0^{(k)} a_0^{(l)}}{a_1^3} \right. \\ & \left. - \frac{a_0^{(k)} a_1^{(l)} + a_0^{(l)} a_1^{(k)}}{a_1^2} \right], \end{aligned} \quad (\text{B9})$$

where the coefficients are explicitly given by

$$\begin{aligned} a_0^{(1)} &= -i \left(\frac{\gamma}{8} - \frac{\epsilon_{\Delta}}{4} \right) \Omega^2, \\ a_0^{(2)} &= -i \left(\frac{\gamma}{8} + \frac{\epsilon_{\Delta}}{4} \right) \Omega^2, \\ a_0^{(11)} &= \frac{1}{8} \gamma \Omega^2, \\ a_0^{(22)} &= \frac{1}{8} \gamma \Omega^2, \\ a_1 &= \epsilon_{\Delta}^2 + \frac{\gamma^2}{4}, \end{aligned}$$

$$\begin{aligned} a_1^{(1)} &= -i\frac{1}{4}\Omega^2, \\ a_1^{(2)} &= -i\frac{1}{4}\Omega^2, \end{aligned}$$

$$a_2 = \frac{\epsilon_{\Delta}^2}{\gamma} + \frac{5}{4}\gamma. \quad (\text{B10})$$

[1] A. E. Cordero-Borboa and R. Unda-Angeles, Morphology and orientated growth of second-phase precipitates in a eu²⁺-doped equimolar kcl:kbr solid solution: an epifluorescence microscopy study by using the doping ion as a fluorochrome, *Microscopy* **69**, 17 (2020).

[2] V. A. Kazakov, A. G. Razina, A. V. Smirnov, and A. I. Vasilev, Clustering in thin silver films upon heating, *Journal of Physics: Conference Series* **2103**, 012109 (2021).

[3] J. A. Hurlbut, G. R. Kavianian, S. Y. Lee, K. L. Nuttall, S. R. Gentry, and T. L. Hassman, Enzyme activity experiments using a simple spectrophotometer, *J. Chem. Educ.* **54**, 442 (1977).

[4] E. J. Haugen, R. Gautam, A. K. Locke, and A. Mahadevan-Jansen, In vivo raman spectroscopy for real-time biochemical assessment of tissue pathology and physiology, *Nature Protocols* **10**.1038/s41596-025-01274-1 (2026).

[5] L. Ciaffoni, G. Hancock, J. J. Harrison, J.-P. H. van Helden, C. E. Langley, R. Peverall, G. A. D. Ritchie, and S. Wood, Demonstration of a mid-infrared cavity enhanced absorption spectrometer for breath acetone detection, *Anal. Chem.* **85**, 846 (2013).

[6] A. Reyes-Reyes, R. C. Horsten, H. P. Urbach, and N. Bhattacharya, Study of the exhaled acetone in type 1 diabetes using quantum cascade laser spectroscopy, *Anal. Chem.* **87**, 507 (2015).

[7] Y. Zhu, T. Fang, D. Ji, H. Li, J. Chen, and J. Ma, Recent advances and prospects in on-site spectrophotometric nutrient measurement in aquatic ecosystems, *TrAC Trends in Analytical Chemistry* **175**, 117723 (2024).

[8] W. Ma, C. Xing, W. Wang, Q. Zhang, Z. Wang, Y. Yang, and C. Liu, Ozone pollution monitoring using a full-time hyperspectral tomography system for multiple air pollutants, *Nature Communications* **10**.1038/s41467-025-66944-w (2025).

[9] M. Aldén, Spatially and temporally resolved laser/optical diagnostics of combustion processes: From fundamentals to practical applications, *Proceedings of the Combustion Institute* **39**, 1185 (2023).

[10] L. Sooväli, E.-I. Rööm, A. Kütt, I. Kaljurand, and I. Leito, Uncertainty sources in uv-vis spectrophotometric measurement, *Accreditation and Quality Assurance* **11**, 246 (2006).

[11] J. Galbán, S. de Marcos, I. Sanz, C. Ubide, and J. Zuriarrain, Uncertainty in modern spectrophotometers, *Anal. Chem.* **79**, 4763 (2007).

[12] J. Dobilienė, E. Raudienė, and R. Žilinskas, Uncertainty of measurement in spectrometric analysis: A case study, *Measurement* **43**, 113 (2010).

[13] C. Peest, C. Schinke, R. Brendel, J. Schmidt, and K. Bothe, Instrumentation-related uncertainty of reflectance and transmittance measurements with a two-channel spectrophotometer, *Review of Scientific Instruments* **88**, 015105 (2017).

[14] D. Skoog, F. Holler, and S. R. Crouch, *Principal of Instrumental Analysis* (Sunder College Publisher, New York, 2017).

[15] W. Demtröder, *Laser Spectroscopy 1* (Springer Berlin, Heidelberg, 2014).

[16] I. Gazizov, D. Pinto, H. Moser, S. Sam, P. Martín-Mateos, L. O'Faolain, and B. Lendl, Absorption and dispersion: In search of a versatile spectroscopic technique, *Sensors and Actuators B: Chemical* **436**, 137688 (2025).

[17] B. M. Escher, R. L. de Matos Filho, and L. Davidovich, General framework for estimating the ultimate precision limit in noisy quantum-enhanced metrology, *Nature Physics* **7**, 406 (2011).

[18] M. A. Taylor and W. P. Bowen, Quantum metrology and its application in biology, *Physics Reports* **615**, 1 (2016), quantum metrology and its application in biology.

[19] T. Li, F. Li, X. Liu, V. V. Yakovlev, and G. S. Agarwal, Quantum-enhanced stimulated brillouin scattering spectroscopy and imaging, *Optica* **9**, 959 (2022).

[20] X. Zhang, Y. Liu, X. Cao, and D. He, Thermodynamic precision in nonequilibrium critical quantum systems, *Phys. Rev. B* **111**, 235401 (2025).

[21] K. E. Dorfman, S. Asban, B. Gu, and S. Mukamel, Hongou-mandel interferometry and spectroscopy using entangled photons, *Communications Physics* **4**, 49 (2021).

[22] Z. Zhang, X. Zhang, J. Liu, and H. Dong, Quantum-enhanced weak absorption estimation with correlated photons, *Phys. Rev. Lett.* **134**, 133604 (2025).

[23] Z. Zhang, T. Peng, X. Nie, G. S. Agarwal, and M. O. Scully, Entangled photons enabled time-frequency-resolved coherent Raman spectroscopy and applications to electronic coherences at femtosecond scale, *Light: Science and Applications* **11**, 10.1038/s41377-022-00953-y (2022).

[24] J. J. Fan, Z.-Y. Ou, and Z. Zhang, Entangled photons enabled ultrafast stimulated raman spectroscopy for molecular dynamics, *Light: Science and Applications* **13**, 163 (2024).

[25] W. E. Moerner, A dozen years of single-molecule spectroscopy in physics, chemistry, and biophysics, *J. Phys. Chem. B* **106**, 910 (2002).

[26] S. Mukamel, Photon statistics: Nonlinear spectroscopy of single quantum systems, *Phys. Rev. A* **68**, 063821 (2003).

[27] E. Barkai, Y. Jung, and R. Silbey, Theory of single-molecule spectroscopy: Beyond the ensemble average, *Annual Review of Physical Chemistry* **55**, 457 (2004).

[28] I. S. Osad'ko and A. N. Lobanov, Fluctuations in the absorption coefficient of a single molecule at different signal acquisition times, *Optics and Spectroscopy* **99**, 289 (2005).

[29] R. Silbey and R. A. Harris, Variational calculation of the dynamics of a two level system interacting with a bath, *The Journal of Chemical Physics* **80**, 2615 (1984).

[30] R. A. Harris and R. Silbey, Variational calculation of the tunneling system interacting with a heat bath. ii. dynamics of an asymmetric tunneling system, *The Journal of Chemical Physics* **83**, 1069 (1985).

[31] D. Xu and J. Cao, Non-canonical distribution and non-equilibrium transport beyond weak system-bath coupling regime: A polaron transformation approach, *Frontiers of Physics* **11**, 110308 (2016).

[32] Y. Tanimura and R. Kubo, Time evolution of a quantum system in contact with a nearly gaussian-markoffian noise bath, *Journal of the Physical Society of Japan* **58**, 101 (1989), <https://doi.org/10.1143/JPSJ.58.101>.

[33] Y. Tanimura, Numerically “exact” approach to open quantum dynamics: The hierarchical equations of motion (heom), *The Journal of Chemical Physics* **153**, 020901 (2020).

[34] N. Makri and D. E. Makarov, Tensor propagator for iterative quantum time evolution of reduced density matrices. ii. numerical methodology, *The Journal of Chemical Physics* **102**, 4611 (1995).

[35] X. Zhang, X. Cao, and D. He, Quantum thermal choke-like behavior exhibited in a spin-boson model under non-commutative coupling, *Phys. Rev. B* **109**, 245415 (2024).

[36] G. Engelhardt, K. Dorfman, and Z. Zhang, Photon-resolved Floquet theory approach to spectroscopic quantum sensing, *Phys. Rev. A* **112**, 063725 (2025).

[37] H. Cramér, *Mathematical Methods of Statistics* (Princeton University Press, Princeton, 1946).

[38] C. Rao, Information and the accuracy attainable in the estimation of statistical parameters, *Bulletin of Calcutta Mathematical Society* **37**, 81 (1945).

[39] C. Wang, J. Ren, and J. Cao, Optimal tunneling enhances the quantum photovoltaic effect in double quantum dots, *New Journal of Physics* **16**, 045019 (2014).

[40] C. Wang, J. Ren, and J. Cao, Nonequilibrium energy transfer at nanoscale: A unified theory from weak to strong coupling, *Scientific Reports* **5**, 11787 (2015).

[41] J. Liu, C.-Y. Hsieh, C. Wu, and J. Cao, Frequency-dependent current noise in quantum heat transfer: A unified polaron calculation, *The Journal of Chemical Physics* **148**, 234104 (2018).

[42] K. E. Dorfman, D. Xu, and J. Cao, Efficiency at maximum power of a laser quantum heat engine enhanced by noise-induced coherence, *Phys. Rev. E* **97**, 042120 (2018).

[43] G. Engelhardt and J. Cao, Tuning the aharonov-bohm effect with dephasing in nonequilibrium transport, *Phys. Rev. B* **99**, 075436 (2019).

[44] G. Schaller and J. Ablaßmayer, Thermodynamics of the coarse-graining master equation, *Entropy* **22**, 10.3390/e22050525 (2020).

[45] T. Becker, A. Schnell, and J. Thingna, Canonically consistent quantum master equation, *Phys. Rev. Lett.* **129**, 200403 (2022).